Article

Not peer-reviewed version

Preparation and corrosion resistance of Zn-Y_2O_3-Al_2O_3 nanocomposite coatings fabricated via electrodeposition

Xiujuan Feng *, Falong Qiu, SEKOU MOHAMED CONDE, Chengliang Dong Dong *

Posted Date: 16 January 2024

doi: 10.20944/preprints202401.1084.v2

Keywords: Electrodeposition; Zn-Y_2O_3-Al_2O_3; Nanocomposite; Corrosion; Microhardness

Article

Preparation and Corrosion Resistance of Zn-Y_2O_3-Al_2O_3 Nanocomposite Coatings Fabricated Via Electrodeposition

Xiujuan Feng [1,2,3,*], Falong Qiu [1,2,3], Sekou Mohamed Conde [1,2,3] and Chengliang Dong [1,2,3,*]

[1] School of Mines, China University of Mining and Technology, Xuzhou, Jiangsu 221116, China
[2] Rare Earth Research Institute, China University of Mining and Technology, Xuzhou, Jiangsu 221116, China
[3] Mechano Chemistry Research Institute, China University of Mining and Technology, Xuzhou Jiangsu 221116, China
* Correspondence: xjfeng@cumt.edu.cn (X.F.); memail3000@126.com(C.D)

Abstract: This article utilized electrodeposition technology to fabricate Zn and Zn-Y_2O_3-Al_2O_3 composite coatings on Q235 steel plates. The composite coatings were obtained by adding Y_2O_3/Al_2O_3 nanoparticles (0, 5, 10, and 15 g/L) to acidic chloride solutions. This study then examined the impact of these nanoparticles on the microstructure, morphology, microhardness, hydrophobicity, and corrosion resistance of the composite coatings. The results indicate that the addition of the nanoparticles increased the nucleation sites on the surface of the coating, thereby refining the grain size and reducing the roughness of the coating surface. When 10g/L of Y_2O_3 and 10g/L of Al_2O_3 nanoparticles were added, the hardness of the composite coating (369 Hv) was 2.49 times higher than that of the pure Zn coating (148 Hv), which was attributed to the dispersion strengthening and grain refinement effects of the nanoparticles. The corrosion resistance of the Zn and Zn-Y_2O_3-Al_2O_3 composite coatings was studied using linear sweep voltammetry and AC impedance spectroscopy. The addition of the nanoparticles improved the corrosion resistance of the composite coating, and the composite coating prepared in an electrolyte containing 10 g/L of Y_2O_3 and 10 g/L of Al_2O_3 nanoparticles exhibited the best corrosion resistance. Meanwhile, the composite coating exhibited good hydrophobicity, with a contact angle of 120.9°, 1.94 times that of the pure Zn coating (62.2°). The Zn-Y_2O_3-Al_2O_3 nanocomposite coating material has significant potential advantages in the field of steel corrosion.

Keywords: electrodeposition; Zn-Y_2O_3-Al_2O_3; nanocomposite; corrosion; microhardness

1. Introduction

Steel has been widely used worldwide as a building material [1], but, in many cases, steel is prone to corrosion, such as atmospheric corrosion, soil corrosion, and water environment corrosion [2–4]. Since steel corrosion can cause significant damage to human life and property each year [5], it is necessary to implement effective measures to reduce it. Pure Zn coatings have advantages such as corrosion resistance, affordability, and ease of production. For decades, zinc coatings have been widely used to protect steel. These coatings can be applied using electrodeposition or hot dip methods [6,7]. Compared with the hot dip method, the zinc coatings obtained via the electrodeposition method are thinner and have a better surface finish. By selecting appropriate electrodeposition parameters, the surface of Zn coatings can be prepared to have no pores, resulting in a higher corrosion resistance and improved mechanical properties [8,9]. However, the corrosion resistance of pure zinc coatings is limited under conditions such as high temperatures and acidic and alkaline environments. Therefore, in order to enhance the performance of Zn coatings, it is necessary to modify them.

Numerous researchers have found that composite coatings can act as viable substitutes for zinc coatings. At present, composite coatings have been widely studied. Introducing ceramic materials

 doi:10.20944/preprints202401.1084.v2

gives coatings, such as Zn-ZrO_2, Ni-W-SiC, and Zn-Al_2O_3, a higher hardness and resistance to high temperatures and corrosion [10–12]. However, when the introduced materials are reduced to the nanoscale, they exhibit entirely different characteristics. Nanoparticles located at grain boundaries can hinder dislocation slip and recrystallization in crystals, thereby improving the performance of composite coatings [13]. Therefore, nanocomposite coatings have better application prospects. Adding nanocomposite materials to traditional coatings can enhance the corrosion resistance, thermal stability, wear resistance, lubricity, and biocompatibility of the coatings [14–18].

Alumina nanoparticles are gaining growing interest because of their high hardness, stability at high temperatures, and exceptional corrosion resistance. Compared with pure Zn coatings, incorporating Al_2O_3 nanoparticles improves the corrosion resistance of composite coatings [19]. Abdulwahab et al. [20] placed Zn-Ni and Zn-Ni-Al_2O_3, obtained via electrodeposition, in a 200°C oven for heat treatment. The hardness value of the Zn-Ni-Al_2O_3 composite coating increased by 2.89%. The hardness of the Zn-Ni alloy plating layer decreased by 26.67%. These results show that nanometer-sized Al_2O_3 particles can enhance thermal stability and resistance to high-temperature oxidation. Blejan et al. [18] found that the addition of nano-alumina to Zn-Ni significantly improved the corrosion resistance of the composite coating.

In recent years, rare earth materials have gradually been used in new materials and in transforming traditional industries [21]. Rare earth yttrium oxide nanoparticles are widely used in applications such as catalysts, biomedical, electronic devices, high-temperature superconductors, and surface modification due to their excellent corrosion resistance and high-temperature oxidation resistance [22]. Zhang et al. [23] added Y_2O_3 to a Zn matrix via filler bonding. The results showed that the addition of Y_2O_3 improved the corrosion resistance of the alloy. When the Y_2O_3 content was increased to 4wt%, the thickest coating showed the highest level of corrosion resistance. Li et al. [24] used the pulsed electrodeposition method to prepare a nanometer composite plating of Ni-W/TiN-Y_2O_3. The studies indicated that the TiN/Y_2O_3 nanoparticles were dispersed in the coating. Nanocrystalline particles with a particle size ranging from 14 to 17 nm were obtained, significantly enhancing the corrosion and wear resistance of the coating.

There are few reports on the study of incorporating Y_2O_3 nanoparticles into a zinc matrix to enhance the performance of coatings. Meanwhile, the preparation of composite coatings by incorporating nanoscale Y_2O_3 and Al_2O_3 particles into a Zn matrix has not yet been published. In this study, we prepared Zn-Y_2O_3-Al_2O_3 nanocomposite coatings on Q235 steel plates using the co-deposition method. Throughout the entire experimental process, the concentrations of the Y_2O_3 and Al_2O_3 nanoparticles were used as independent variables to investigate their effects on the morphology, corrosion behavior, and mechanical properties of the Zn-Y_2O_3- Al_2O_3 nanocomposite coatings.

2. Materials and Methods

2.1. Preparation of electrolyte solution

The composition of the electroplating bath is described in Table 1. All agents were of analytical purity grade. HCl or NaOH was added to a plating solution to decrease its pH to 3.5. Then, Al_2O_3 (50 nm) and Y_2O_3 (20 nm) particles were added to the plating solution, and a magnetic agitator was used to stir at 1000 rpm for 18 hours to ensure the uniform dispersion of the nanopowders.

Table 1. Bath composition and operating conditions.

Composition	Concentration (g/L)	Parameters	
$ZnCl_2$	150	Temperature (°C)	25
KCl	50	pH	3.5
Boric acid	30	Plating time (min)	60
Al_2O_3	0-15		
Y_2O_3	0-15		

 doi:10.20944/preprints202401.1084.v2

2.2. Pretreatment of substrate

In this work, the anode was a 15×10×1 mm^3 zinc sheet (purity 99.999 %), and the substrate (cathode) was Q235 carbon steel, with a size of 10×10×1 mm^3. Since the purchased carbon steel surface had scratches, rusting, and other defects, it was necessary to preserve its surface. Thus, 400, 800, 1200, 1600, 2000, and 3000 grit emery papers were used to grind the surface of the carbon steel and remove surface impurities and the oxidation layer; then, it was polished with a w3.5 abrasive paste. After achieving a flawless surface, the samples were placed in a drier. To remove the grease from the carbon steel surface, it was placed in ethanol and subjected to ultrasonic cleaning for 15 min. The washed samples were soaked for 15 seconds in a 1 M HNO_3 solution. This activation step aimed to eliminate the oxidation layer formed on the surface of the carbon steel and enhance the coating quality. After activation, the substrate was rinsed with deionized water and then left to air dry.

2.3. Preparation of composite coatings

Figure 1 shows a schematic diagram of the experimental setup for electrodeposition. In this experiment, the anode used epoxy resin to embed the five sides of the carbon steel sheet, leaving only a 1 cm^2 area exposed, and it was connected with a copper wire. The electrodeposition experiment co-deposited for 1 h with a 30 mA/cm^2 current density at 35°C. The electroplating solution was stirred constantly with a magnetic agitator at a rate of 550 rpm during the experiment to keep the nanoparticles suspended in the solution at all times. Once the experiment was complete, the sample was flushed with deionized water for 10 seconds and then left to dry. The Y_2O_3 and Al_2O_3 content in the plating solution determined the composition of the deposited Zn-Y_2O_3-Al_2O_3 composite coating. The coating descriptions are shown in Table 2.

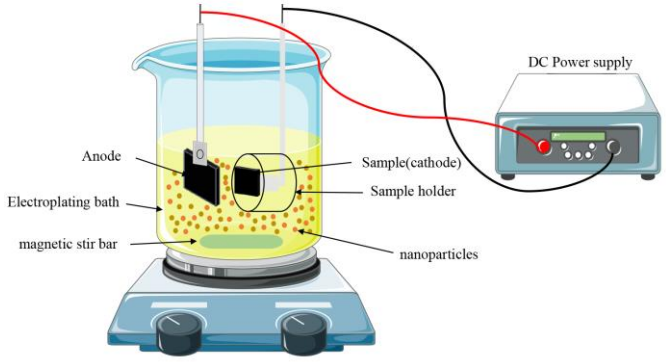

Figure 1. Schematic diagram of the experimental setup.

Table 2. Simple codes and descriptions.

Simple codes	Simple descriptions
C1	Zn
C2	Zn-5g/L Y_2O_3-5g/L Al_2O_3
C3	Zn-10g/L Y_2O_3-10g/L Al_2O_3
C4	Zn-15g/L Y_2O_3-15g/L Al_2O_3

2.4. Surface characterization

The surface morphology of the composite coating was analyzed using environmental scanning electron microscopy (ESEM, USA). An X-ray diffractometer (XRD, DMAX, Riken Instruments Japan) operated with Cu-Kα radiation was used to analyze the phase structures of the composite coatings. The scanning rate was set to 5°/min, and the scanning range was $10° < \theta < 90°$.

 doi:10.20944/preprints202401.1084.v2

2.5. Electrochemical measurement

Using an electrochemical workstation (Admiral, USA), electrochemical impedance spectroscopy (EIS) and linear sweep voltammetry (LSV) tests were conducted in a three-electrode system to evaluate the corrosion behavior of the composite coatings. The three-electrode system consisted of a composite coating as the working electrode, Ag/AgCl as the reference electrode, and a platinum plate electrode with a working area of 1 cm^2. Before conducting the testing study, the coating samples were immersed in a 3.5wt% NaCl solution for a specific period to obtain a stable open-circuit potential (OCP). The linear sweep voltammetry test was conducted in a 3.5wt% NaCl electrolyte, with a potential range of -1.5 V~1.5 V and a scanning rate of 10 mV/s. The measurement of EIS ranged from 0.1 Hz to 100000 Hz, with a disturbance voltage of 10 mV.

2.6. Microhardness test

A microhardness tester (VH1102, China) was used to test the hardness of the composite coatings. The applied load was 50 g, and the loading time was 10 seconds. Ten points were selected on the surface of each composite coating for hardness testing, and the average value was taken.

2.7. Contact angle text

The static contact angle of the coating was measured using a contact angle detector (JY-PHb, China). At 25°C, the contact angle was measured on the surface of the coating by using 3 μL of deionized water droplets. The surface coating was tested at ten different locations to minimize experimental errors, and the average value was calculated as the final value.

3. Results and discussion

3.1. Deposition mechanism of nanocomposite coatings

The formation mechanism of the nanocomposite coatings is shown in Figure 2. When a stable voltage is applied to both ends of the electrode, Zn^{2+} in the solution migrates towards the cathode. At the cathode, electrons are gained, and an oxidation–reduction reaction occurs, forming Zn nuclei on the cathode's surface. At the same time, H^+ in the solution combines with electrons to form H_2, while OH^- near the anode (Zn sheet) loses electrons and produces O_2. During this process, the nanoparticles dispersed in the plating solution adsorb with Zn^{2+} and migrate towards the cathode surface. Upon reaching the cathode, they adsorb onto the metal surface to form a diffusion layer. When Zn^{2+} undergoes oxidation–reduction to form a Zn coating, the nanoparticles adsorbed by Zn^{2+} are embedded into the Zn coating, ultimately forming a nanocomposite coating. The reaction equations are as follows [25]:

Cathode:

$$Zn^{2+} + 2e^- \rightarrow Zn \quad (1)$$

$$2H^+ + 2e^- \rightarrow H_2 \uparrow \quad (2)$$

Anode:

$$Zn - 2e^- \rightarrow Zn^{2+} \quad (3)$$

$$4OH^- + 4e^- \rightarrow 2H_2O + O_2 \uparrow \quad (4)$$

 doi:10.20944/preprints202401.1084.v2

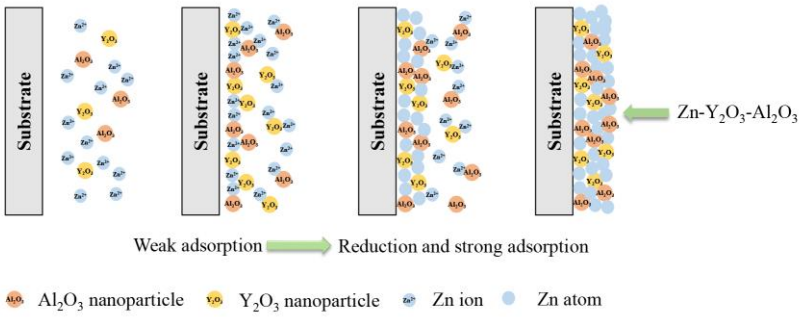

Figure 2. Diagram of mechanism of coating preparation using electrodeposition method.

3.2. X-ray diffraction (XRD)

Figure 3 presents an X-ray diffraction (XRD) pattern of the Zn coating and the Zn-Y_2O_3- Al_2O_3 coating with varying nanoparticle concentrations. Most of the diffraction lines in the X-ray diffraction pattern correspond to the hexagonal structure of Zn[11]. The Zn-Y_2O_3-Al_2O_3 nanocomposite coating had a similar structure to the zinc coating, but the preferential orientation of Zn changed. The diffraction diagram shows six distinct peaks at 36.6°, 43.5°, 54.6°, 70.3°, 77.3°, and 82.4° on standard PDF cards, corresponding to the Zn phase (002), (101), (102), (110), (004), and (112) planes. As depicted in the graph, the addition of the Y_2O_3 and Al_2O_3 nanoparticles resulted in a significant increase in (002) crystal diffraction peaks. The intensity of most of the remaining diffraction peaks weakened, indicating that the introduction of nanoparticles further enhanced the deposition orientation of the (002) crystal surface. Low-intensity Al_2O_3 peaks were observed in all XRD profiles of the Zn-Y_2O_3-Al_2O_3 coatings at 35.02 °, 57.86 °, and 65.89 °. This proves the successful co-deposition of the Al_2O_3 nanoparticles with the zinc matrix. At the same time, the low-intensity peaks of Zn-Y_2O_3-Al_2O_3 were observed in all XRD profiles of the Y_2O_3 coatings XRD at 28.70°, 48.19°, and 57.29°. It was also proven that the Y_2O_3 nanoparticles were successfully added to the zinc matrix. In addition, the peak width of the Zn-Y_2O_3-Al_2O_3 nanocomposite coating was slightly wider than that of the Zn coating. This is because the nanoparticles inhibited the growth of the crystals, resulting in the refinement of the crystal size[10].

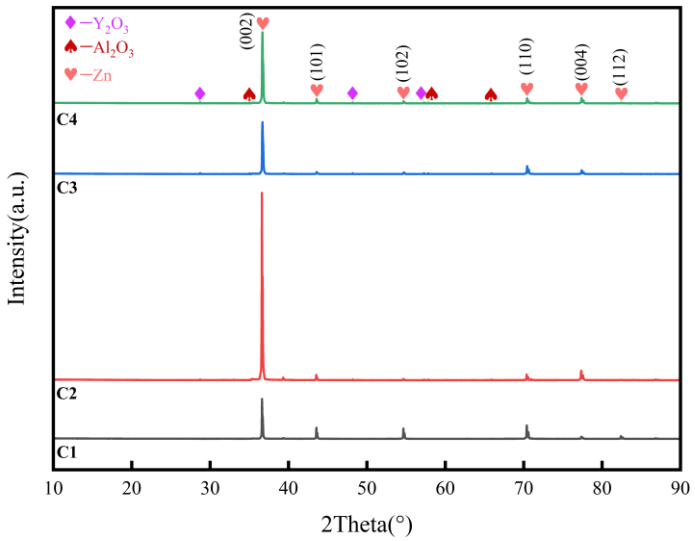

Figure 3. XRD patterns of Zn coating and Zn-Y_2O_3-Al_2O_3 coating.

 doi:10.20944/preprints202401.1084.v2

3.3. Surface morphology of composite coatings

Figure 4 shows the surface shapes of the Zn-Y_2O_3-Al_2O_3 coatings obtained by adding different concentrations of nanometer Y_2O_3 and Al_2O_3 particles to electrolytes. As can be seen in the diagram, the surface of the pure zinc coating exhibits a flake crystal structure, which is observed to be unevenly distributed. The microstructure of the C3 coating is significantly better than that of the pure C1, C2, and C4 coatings, mainly in its dense organization and small grain size. The microstructure refinement of the composite coatings is mainly due to the introduction of nanoparticles, which are successfully and uniformly dispersed and encapsulated in the Zn matrix. The nanoparticles bound to the Zn matrix increase the number of nucleation sites, impede the growth of crystals, and lead to the formation of small-sized grains. The surface of the C2 coating exhibits a partially dense microstructure and smaller grains. This can be attributed to the low concentration of incorporated nanoparticles, which reduces nucleation sites on the coating surface [15]. The surface of the C4 coating is rough, the grain size is large, and there are cracks and holes. This may be due to an excessive concentration of added nanoparticles. This results in the agglomeration of nanoparticles and increased stress within the composite coating [26]. A reduced grain size and a dense microstructure are always ideal for composite coatings with a high hardness and excellent corrosion resistance [27].

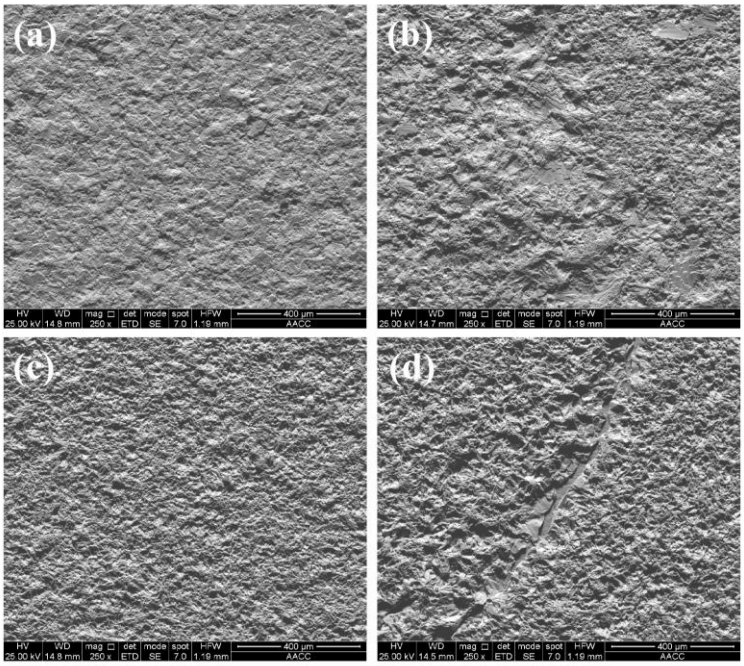

Figure 4. SEM images of Zn-Y_2O_3-Al_2O_3 coatings obtained from the deposition of different nanometer Y_2O_3 and Al_2O_3 concentrations in electrolytes: (a) C1, (b) C2, (c) C3, (d) C4.

3.4. Effect of particle loading on corrosion resistance

The open-circuit potential refers to the potential difference between a soluble metal electrode and an electrolyte due to the spontaneous redox reaction that occurs when the electrode is immersed in the electrolyte. The system is in a dynamic equilibrium at an open-circuit potential. This means that the redox reaction occurring on the electrode and the reaction in the electrolyte are in equilibrium, and the electrode does not undergo significant corrosion. Figure 5a illustrates the change in the open-circuit potential of the pure Zn and Zn-Y_2O_3-Al_2O_3 composite coatings over time in a 3.5wt% NaCl solution. As shown in the figure, compared with the pure Zn coating, the composite coating exhibits a higher potential. This suggests that the composite coating performs better because it suppresses the anodic reaction and enhances the composite coating's anti-corrosion properties.

The corrosion behavior of various composite coatings was studied using linear scanning voltammetry. Figure 5b shows a polarization curve of the Zn-Y_2O_3-Al_2O_3 composite coating in a 3.5wt% NaCl solution with various concentrations of Y_2O_3 and Al_2O_3 nanoparticles. The self-

 doi:10.20944/preprints202401.1084.v2

corrosion current (I_{coor}) and corrosion voltage (E_{coor}) fitted according to Tafel extrapolation are listed in Table 3. In general, the higher the positive corrosion potential of the coating, the lower the self-corrosion current density, indicating that the coating has a lower tendency to corrode [28]. As shown in Table 3, the corrosion potential of the composite coatings is higher than that of the pure zinc coatings (E_{coor}=1.18 V). This demonstrates that the Zn coating's resistance to corrosion can be effectively increased by using nanoscale Y_2O_3 and Al_2O_3 particles. A plating solution containing 10 g/L of Y_2O_3 and Al_2O_3 nanoparticles raises the composite coating's corrosion potential to 1.02 V. Meanwhile, the self-corrosion current density of the Zn-Y_2O_3-Al_2O_3 nanocomposite coating (I_{coor}=6.15×10^{-6}) is significantly lower than that of the other coatings. From the perspective of corrosion kinetics, the corrosion rate of the nanocomposite coatings is slower than that of the pure Zn coatings.

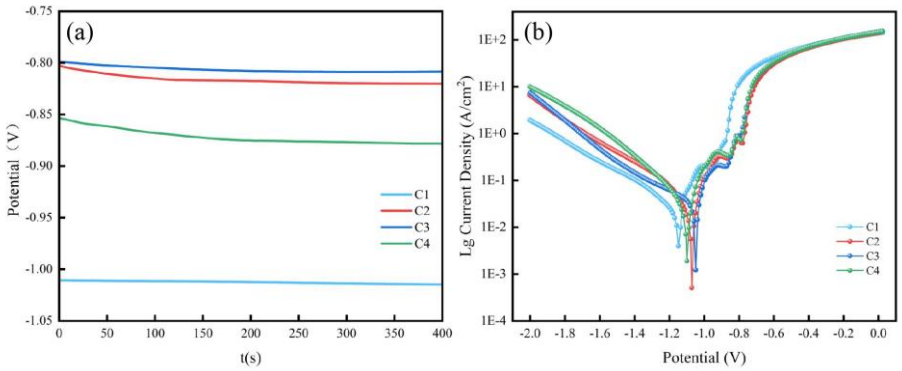

Figure 5. (a) Open-circuit potential of Zn and Zn-Y_2O_3-Al_2O_3 composite coatings immersed in 3.5wt% NaCl solution varies with time. (b) Tafel curves of zinc and Zn-Y_2O_3-Al_2O_3 composite coatings in 3.5wt% NaCl solution.

Table 3. Corrosion parameters of Zn-Y_2O_3-Al_2O_3 composite coating in 3.5wt% NaCl solution.

Sample	E_{corr} (V)	I_{corr} (A/cm²)
C1	-1.18	6.64×10^{-5}
C2	-1.07	3.28×10^{-5}
C3	-1.02	6.15×10^{-6}
C4	-1.10	3.91×10^{-5}

Figure 5b shows that the current density of the Zn coating reduces as the reaction progresses in the cathode polarization region, covering a range from -2.0 V to -1.18 V. This is because electrons are attracted from the solution to the electrode surface and react with oxygen in the following manner:

$$2H_2O + O_2 + 2e^- = 4OH^- \quad (5)$$

When located in the anode polarization region from -1.18 V to 0.7 V, the current density of the Zn coating increases as the reaction progresses. This occurs when the coating begins to react with the electrolyte, primarily through the following reaction:

$$Zn(s) = Zn^{2+} + 2e^- \quad (6)$$

However, as the reaction progresses, the change in current density stabilizes when the scanning potential increases above 0.7 V. The stability exhibited can be attributed to the creation of an oxide-based passivation film on the surface of the coating, which impedes the rate of coating dissolution [29]. The formation of this film primarily occurs as follows:

$$Zn^{2+} + 2OH^- = Zn(OH)_2 \quad (7)$$

$$2Zn + O_2 = 2ZnO \quad (8)$$

In addition, particle agglomeration reduces its usability, resulting in reduced co-deposition efficiency and the formation of low-quality coatings [30]. When the concentration of these

 doi:10.20944/preprints202401.1084.v2

nanoparticles in the electroplating solution is increased from 0 g/L to 15 g/L, the corrosion current density of the composite coating follows a pattern of initially decreasing and then increasing. When the nanoparticles are incorporated at a concentration of 10 g/L, the nanocomposite coatings exhibit minimal corrosion current density, indicating optimal corrosion resistance. The optimal particle load for achieving this resistance is 10 g/L of nanometer Y_2O_3 and 10 g/L of nanometer Al_2O_3. The particles in the electroplating solution are dispersed at the optimum level at this concentration. Via the formation of these nanoparticles, an inert physical barrier is established on the coating's surface, which reduces the effective contact area between the corrosive medium and the substrate metal, improving the coating's corrosion resistance [13].

Electrochemical impedance spectroscopy is a powerful electrochemical auxiliary technique commonly used to evaluate the corrosion resistance of prepared coating surfaces [31]. AC impedance testing was conducted on the prepared composite coatings to investigate their corrosion resistance further in a 3.5wt% NaCl solution. Figure 6a shows Nyquist plots of the different composite coatings obtained through EIS testing. It can be seen in the figure that a single capacitive ring with a circular arc shape is displayed from high frequency to low frequency. A relationship exists between the radius of the capacitive impedance arc and the charge transfer resistance, where a larger arc radius signifies a higher charge transfer resistance value and improved corrosion resistance performance of the coating [32]. The impedance arc radius of the composite coating exhibits a trend of initially increasing and then decreasing as the doping concentrations of the Y_2O_3 and Al_2O_3 nanoparticles are increased. The composite coating exhibits the largest impedance arc and superior corrosion resistance at a doping concentration of 10g/L for both the Y2O3 and Al2O3 nanoparticles. This finding aligns with the polarization curve test results of the composite coating. The Randles circuit model was used for fitting to explain the EIS results further, and the equivalent circuit is shown in Figure 6b, characterized by only one time constant [33]. Within this equivalent circuit, R_s denotes the resistance of the electrolyte. CPE is a constant-phase angle element, and a lower CPE value signifies a higher surface quality of the composite coating [34]. R_{ct} stands for charge transfer resistance, which is associated with the corrosion rate and serves as a crucial parameter reflecting the corrosion resistance of composite coatings. A higher R_{ct} value indicates superior corrosion resistance of the composite coating. The fitting data for the coatings are presented in Table 4, revealing that the maximum impedance modulus of all composite coatings exceeds that of the pure Zn coatings (1385 Ω cm^2). The impedance modulus reaches a remarkable value of 10257 Ω cm^2 for the C3 coating, indicating its exceptional corrosion resistance.

Table 4. Impedance spectrum fitting results of different samples.

Sample	R_s (Ω cm^2)	R_{ct} (Ω cm^2)	CPE-P	CPE-T
C1	4.781	1385	0.912	1.26×10^{-4}
C2	4.678	2304	0.840	4.79×10^{-4}
C3	4.539	10257	0.823	6.59×10^{-4}
C4	4.384	6622	0.859	2.11×10^{-4}

Figure 6c shows a Bode modulus diagram, and | Z | represents the impedance value of the composite coating. The impedance modulus in the low-frequency zone is frequently used to assess the corrosion resistance of coatings. This is because the formation of a protective barrier, such as the corrosion product film, at the steel/coating interface effectively mitigates corrosion [35–37]. When the doping concentrations of the Y_2O_3 and Al_2O_3 nanoparticles are both 10 g/L, the highest impedance value in Figure 6c is 6592.84 Ω cm^2, indicating that the C3 coating has a better corrosion resistance. In addition, at higher frequencies, a larger phase angle indicates the presence of a more stable dielectric film, and the stability of the coating is also better [38]. The maximum phase angle of the C3 coating indicates that it has a better stability and better barrier performance.

 doi:10.20944/preprints202401.1084.v2

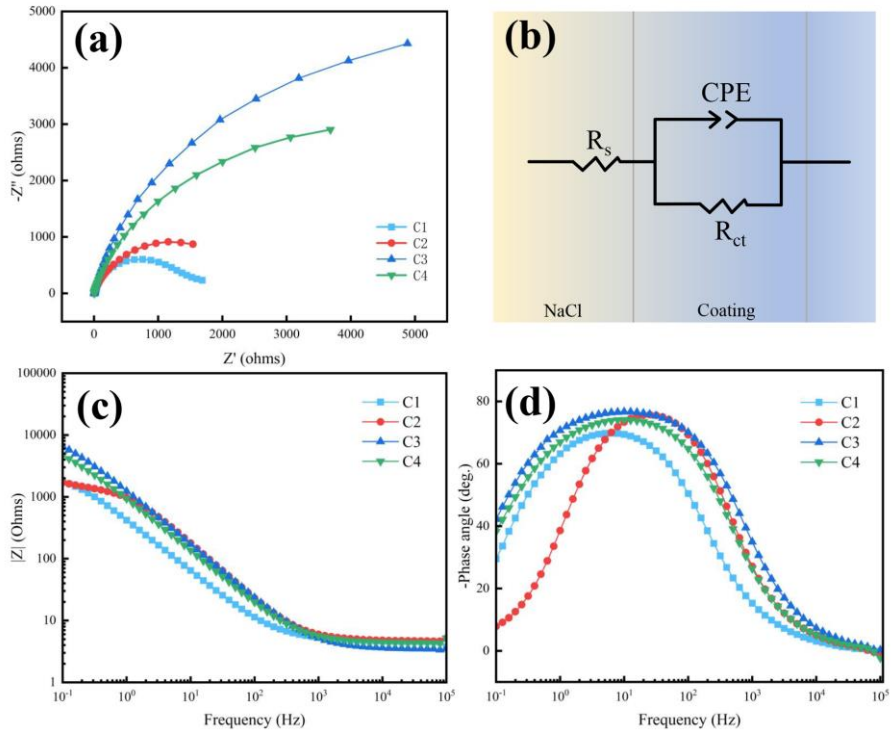

Figure 6. Zn and Zn-Y_2O_3-Al_2O_3 composite coatings in a 3.5wt% NaCl solution. (a) Nyquist diagram. (b) Equivalent circuit model. (c) Bode modulus diagram. (d) Bode-phase diagram.

3.5. Microhardness test

In practice, coatings not only require excellent corrosion resistance but also excellent mechanical properties. Therefore, the mechanical properties of the Zn and Zn-Y_2O_3-Al_2O_3 coatings are evaluated via microhardness testing. To mitigate experimental error, ten points are randomly chosen from each sample for hardness testing. The average value of these points is considered the sample's hardness result.

The hardness test results for the Zn and Zn-Y_2O_3-Al_2O_3 coatings are shown in Figure 7. Based on the graph, it is observable that the composite coating exhibits a higher microhardness than the pure Zn coating. As the content of Y_2O_3 and Al_2O_3 nanoparticles increases in the plating solution, the hardness of the composite coating initially increases and then decreases. The pure zinc coating has a hardness value of 148 Hv. However, when 10 g/L of nanoscale Y_2O_3 and Al_2O_3 particles is added, the hardness of the composite coating reaches 369 Hv, indicating a 2.5-fold increase compared to the pure Zn coating. The inclusion of nanoparticles significantly enhances the microhardness of the composite coating [39]. However, this is due to the excellent mechanical properties of the Y_2O_3 and Al_2O_3 nanoparticles, which are uniformly dispersed in the Zn matrix, playing a dispersion-strengthening role. However, nanoparticles bound to the Zn matrix increase the number of nucleation sites. In addition, they hinder crystal growth, resulting in the formation of small grain sizes and promoting a significant number of grain boundaries [18,40]. The coating surface is dense, and this grain refinement helps to increase the hardness value of the coating [41]. With a 15 g/L concentration of the Y_2O_3 and Al_2O_3 nanoparticles in the plating solution, the hardness of the coating decreases. This is due to the pronounced agglomeration behavior of the nanoparticles, leading to the formation of uneven areas, such as pores and cracks, on the surface of the composite coating. As a result, the dispersion-strengthening effect of the nanoparticles within the coating diminishes, causing a reduction in the hardness value of the composite coating.

 doi:10.20944/preprints202401.1084.v2

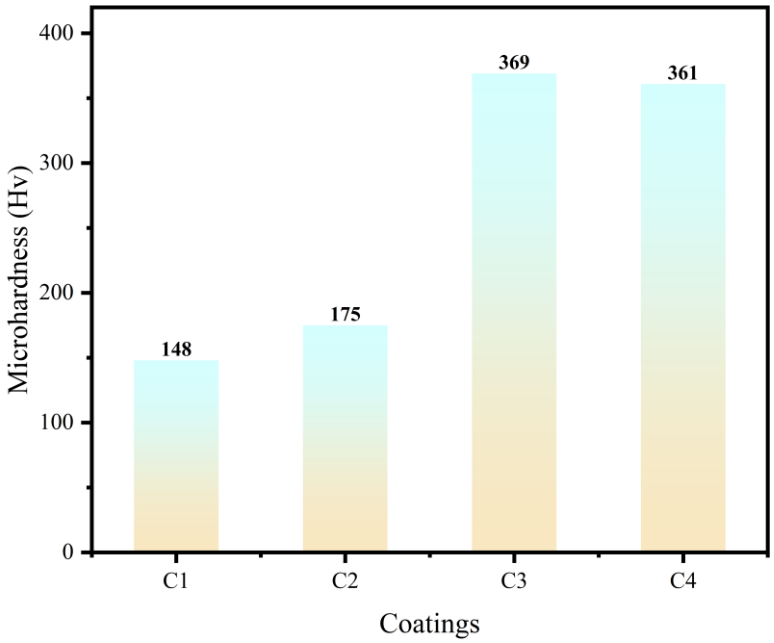

Figure 7. Microhardness of different coatings.

3.6. Contact angle text

Variations in the surface morphology of Zn coatings can lead to differences in hydrophobic properties [42]. Figure 8 presents the static contact angle (CA) of the Zn-Y_2O_3-Al_2O_3 composite coating in deionized water with various doping concentrations of the Y_2O_3 and Al_2O_3 nanoparticles. The figure shows that the CA of the pure zinc coating is 62.2°, while the CA of the composite coating surpasses that of the pure Zn coating. As the doping concentration of the nanometer Y_2O_3 and Al_2O_3 particles increases, the CA of the composite coating initially exhibits an increase, followed by a decrease. In addition, when the Y_2O_3 and Al_2O_3 nanoparticles were added to the plating solution at a concentration of 10 g/L, the composite coating obtained had a maximum CA of about 120.9°, indicating excellent hydrophobic properties. The surface hydrophobicity test results for the composite coating align with the findings of the corrosion resistance assessment. This is because the non-uniform nanostructure present on the composite coating surface traps a significant volume of air within the material, leading to a considerable reduction in the contact area and contact duration between the coating surface and the corrosive medium. When the coating is submerged in a corrosive medium, the gas trapped on the coating's surface creates a protective gas film between the corrosive medium and the metal surface, thereby enhancing the corrosion resistance of the hydrophobic coating within the corrosive environment [43].

 doi:10.20944/preprints202401.1084.v2

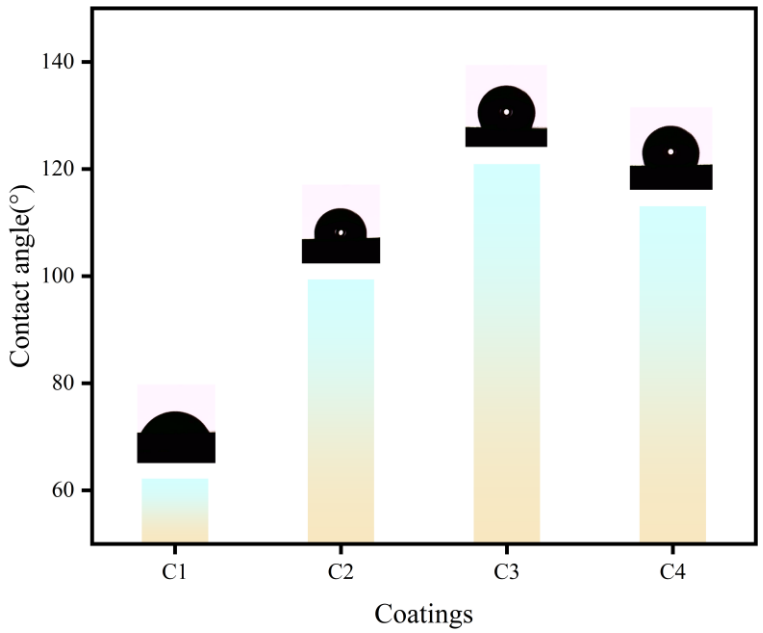

Figure 8. Contact angles of the different coatings.

4. Conclusions

In this paper, a Zn-Y_2O_3-Al_2O_3 nanocomposite coating is successfully prepared on a Q235 steel plate using electrodeposition technology. This is achieved by adding nanoparticles to a plating solution. This research examines the impact of nanoparticles on the surface morphology, microhardness, hydrophobicity, corrosion, and resistance of composite materials. The findings suggest that the incorporation of nanoparticles augments the number of nucleation sites on the coating surface, impedes crystal growth, accomplishes grain refinement, and diminishes surface roughness. Due to grain refinement and the strengthening of dispersion, the hardness of the Zn-Y_2O_3-Al_2O_3 nanocomposite coatings is significantly improved. According to the research, the composite coating demonstrates favorable hydrophobicity and exceptional corrosion resistance at a nanoparticle dosage of 10 g/L. This can be attributed to the formation of an inert physical barrier on the coating surface by the nanoparticles. This barrier significantly reduces the contact time and surface area between the coating and the corrosive medium, effectively isolating the corrosive medium from the Q235 steel plate.

Author Contributions: Conceptualization, X.F.; methodology, X.F., F.Q., S.M.C., and C.D.; validation, F.Q.; formal analysis, F.Q.; investigation, X.F., F.Q., S.M.C., and C.D.; resources, X.F.; data curation, X.F. and F.Q.; writing—original draft, F.Q.; writing—review and editing, X.F. and S.M.C.; visualization, F.Q.; supervision, X.F.; project administration, X.F. and C.D.; funding acquisition, X.F. All authors have read and agreed to the published version of the manuscript.

Funding: This work was supported by the National Key R&D Program of China (Grant No. 2021YFC2902100), the Postgraduate Research & Practice Innovation Program of Jiangsu province (Grant No. KYCX23_2810), and the Graduate Innovation Program of China University of Mining and Technology (Grant No. 2023WLJCRCZL039).

Institutional Review Board Statement: Not applicable.

Informed Consent Statement: Not applicable.

Data Availability Statement: Not applicable.

Conflicts of Interest: The authors declare no conflicts of interest.

Abbreviations

The following abbreviations are used in this manuscript:

LSV	Linear sweep voltammetry
EIS	Electrochemical impedance spectroscopy
OCP	Open-circuit potential
CA	Contact angle

References

1. Zou, Y.; Wang, J.; Zheng, Y. Y. Electrochemical techniques for determining corrosion rate of rusted steel in seawater. *Corros. Sci.* **2011,** 53, (1), 208-216.
2. Lin, C. C.; Wang, C. X. Correlation between accelerated corrosion tests and atmospheric corrosion tests on steel. *J. Appl. Electrochem.* **2005,** 35, (9), 837-843.
3. Choi, Y. S.; Nesic, S.; Young, D. Effect of impurities on the corrosion behavior of CO_2 transmission pipeline steel in supercritical CO_2-water environments. *Environ. Sci. Technol.* **2010,** 44, (23), 9233-9238.
4. Wang, S.; Du, C.; Li, X.; Liu, Z.; Zhu, M.; Zhang, D. Field corrosion characterization of soil corrosion of X70 pipeline steel in a red clay soil. *Prog. Nat. Sci.: Mater. Int.* **2015,** 25, (3), 242-250.
5. Chen, B.; Wu, Q.; Li, J.; Lin, K.; Chen, D.; Zhou, C.; Wu, T.; Luo, X.; Liu, Y. A novel and green method to synthesize a epoxidized biomass eucommia gum as the nanofiller in the epoxy composite coating with excellent anticorrosive performance. *Chem. Eng. J.* **2020,** 379.
6. Basavanna, S.; Naik, Y. A. Electrochemical studies of Zn-Ni alloy coatings from acid chloride bath. *J. Appl. Electrochem.* **2009,** 39, (10), 1975-1982.
7. Popoola, A. P. I.; Fayomi, O. S. Performance evaluation of zinc deposited mild steel in chloride medium. *Int. J. Electrochem. Sci.* **2011,** 6, (8), 3254-3263.
8. Elsherief, A. E.; Shoeib, M. A. Characterization of electro-deposited Zn-Ni alloy from an all-chloride solution. *Corros. Prev. Control* **2003,** 50, (1), 25-34.
9. Amuda, M. O. H.; Subair, O. W.; Obitayo, O. W. Study of optimum conditions for zinc plating on mild steel. *Int. J. Eng. Res. Afr.* **2010,** 2, 31-39.
10. Vathsala, K.; Venkatesha, T. V. Zn-ZrO_2 nanocomposite coatings: Elecrodeposition and evaluation of corrosion resistance. *Appl. Surf. Sci.* **2011,** 257, (21), 8929-8936.
11. Malatji, N.; Popoola, A. P. I.; Fayomi, O. S. I.; Loto, C. A. Multifaceted incorporation of Zn-Al_2O_3/Cr_2O_3/SiO_2 nanocomposite coatings: anti-corrosion, tribological, and thermal stability. *Int. J. Adv. Manuf. Technol.* **2016,** 82, (5-8), 1335-1341.
12. Zhang, P.; Zhao, Y.; Huang, J.; Li, J.; Cao, L.; Liu, J.; Han, G.; Du, W.; Chen, L.; Xiao, L.; Wang, Q.; Yang, Y.; Zhu, S.; Li, W. Enhanced mechanical and wear properties of Ni-W-SiC composite coatings by synergistic influence of micro-nano SiC mixture. *Surf. Coat. Technol.* **2023,** 467.
13. Jin, X.; Wang, J.; Wang, S.; Cao, Y.; Fang, A.; Wang, Q.; Gong, J.; Dai, Y. Fabrication of Pb-Co-ZrO_2 nanocomposite coatings and correlation of corrosion mechanisms with electronic work functions. *Mater. Today Commun.* **2023,** 37.
14. Fustes, J.; Gomes, A.; da Silva Pereira, M. I. Electrodeposition of Zn-TiO_2 nanocomposite films-effect of bath composition. *J. Solid State Electrochem.* **2008,** 12, (11), 1435-1443.
15. Praveen, B. M.; Venkatesha, T. V. Electrodeposition and properties of Zn-nanosized TiO_2 composite coatings. *Appl. Surf. Sci.* **2008,** 254, (8), 2418-2424.
16. Zheng, H.-Y.; An, M.-Z. Electrodeposition of Zn-Ni-Al_2O_3 nanocomposite coatings under ultrasound conditions. *J. Alloys Compd.* **2008,** 459, (1-2), 548-552.
17. Ranganatha, S.; Venkatesha, T. V.; Vathsala, K.; Kumar, M. K. P. Electrochemical studies on Zn/nano-CeO_2 electrodeposited composite coatings. *Surf. Coat. Technol.* **2012,** 208, 64-72.
18. Blejan, D.; Muresan, L. M. Corrosion behavior of Zn-Ni-Al_2O_3 nanocomposite coatings obtained by electrodeposition from alkaline electrolytes. *Mater. Corros.* **2013,** 64, (5), 433-438.
19. Malatji, N.; Popoola, A. P. I.; Fayomi, O. S. I. The effect of nanoparticulate loading on the fabrication and characterization of multi-doped Zn-Al_2O_3-Cr_2O_3 hybrid coatings on mild steel. *Int. J. Adv. Manuf. Technol.* **2017,** 90, (9-12), 2443-2452.
20. Abdulwahab, M.; Fayomi, O. S. I.; Popoola, A. P. I.; Dodo, M. R. In-situ hybrid study of thermal behaviour of Zn-Ni and Zn-Ni-Al2O3 nanocrystallite thin films induced TEA/MEA by electrocodeposition. *Results Phys.* **2017,** 7, 213-215.
21. Harvey, T. G. Cerium-based conversion coatings on aluminium alloys: A process review. *Corros.Eng.Sci.Technol.* **2013,** 48, (4), 248-269.
22. Xing, S.; Zhu, W.; You, S.; Yu, W.; Jiang, C.; Ji, V. Investigation on microstructure and tribological performances of electrodeposited Ni-W-Y_2O_3 composite coatings. *J. Alloys Compd.* **2023,** 965.

23. Zhang, Y. J.; Wang, Z. X.; Yu, R. P.; Zhao, H. Effect of Adding Y_2O_3 on Property of Zn Coatings via Pack Cementation. *Surf. Eng. Appl. Electrochem.* **2023,** 59, (2), 192-198.
24. Li, B.; Li, D.; Zhang, J.; Chen, W.; Zhang, W. Electrodeposition of Ni-W/TiN-Y_2O_3 nanocrystalline coating and investigation of its surface properties and corrosion resistance. *J. Alloys Compd.* **2019,** 787, 952-962.
25. Safavi, M. S.; Tanhaei, M.; Ahmadipour, M. F.; Ghaffari Adli, R.; Mahdavi, S.; Walsh, F. C. Electrodeposited Ni-Co alloy-particle composite coatings: A comprehensive review. *Surf. Coat. Technol.* **2020,** 382.
26. Wu, T.; Ma, M.; Ding, K.; Nan, X.; Wang, Z.; Wei, X.; Zhu, X. Effect of Y_2O_3 nanoparticles on the microstructure and corrosion resistance of electrodeposited Ni-Mo-Y2O3 nanocomposite coatings. *Int. J. Electrochem. Sci.* **2023,** 18, (6).
27. Kumar, C. M. P.; Chandrashekarappa, M. P. G.; Kulkarni, R. M.; Pimenov, D. Y.; Giasin, K. The Effect of Zn and Zn-WO_3 Composites Nano-Coatings Deposition on Hardness and Corrosion Resistance in Steel Substrate. *MATERIALS* **2021,** 14, (9).
28. Jin, W.; Xiao, S.; Kou, Q.; Ding, D.; Zhang, J.; Fang, X.; Ge, C.; Zhong, C.; Zhu, H.; Haarberg, G. M. Preparation of diboride coatings by electrophoretic deposition in nanoparticle-containing molten inorganic salts. *Mater. Lett.* **2022,** 306.
29. Bakhit, B.; Akbari, A.; Nasirpouri, F.; Hosseini, M. G. Corrosion resistance of Ni-Co alloy and Ni-Co/SiC nanocomposite coatings electrodeposited by sediment codeposition technique. *Appl. Surf. Sci.* **2014,** 307, 351-359.
30. Ridosic, M.; Salicio-Paz, A.; Garcia-Lecina, E.; Zabinski, P.; Zivkovic, L. S.; Bajat, J. B. The effect of the ultrasound agitation and source of ceria particles on the morphology and structure of the Zn-Co-CeO_2 composite coatings. *J.MATER.RES.TECHNOL.* **2021,** 13, 1336-1349.
31. Liu, Y.; Li, S.; Zhang, J.; Liu, J.; Han, Z.; Ren, L. Corrosion inhibition of biomimetic super-hydrophobic electrodeposition coatings on copper substrate. *Corros. Sci.* **2015,** 94, 190-196.
32. He, X.; Song, R. G.; Kong, D. J. Microstructure and corrosion behaviours of composite coatings on S355 offshore steel prepared by laser cladding combined with micro-arc oxidation. *Appl. Surf. Sci.* **2019,** 497.
33. Du, Y.; Wang, D.; Si, P.; Wei, L.; Wang, Y.; Yu, B.; Zhang, X.; Ye, S. Electrodeposition of a Ni-P-$Ti_3C_2T_x$/MoS_2 coating incorporating MoS_2 intercalated $Ti_3C_2T_x$ particles. *Surf. Coat. Technol.* **2018,** 354, 119-125.
34. Ren, A.; Kang, M.; Fu, X. Corrosion behaviour of Ni/WC-MoS_2 composite coatings prepared by jet electrodeposition with different MoS_2 doping concentrations. *Appl. Surf. Sci.* **2023,** 613.
35. Ma, Y.; Zhang, Y.; Liu, J.; Ge, Y.; Yan, X.; Sun, Y.; Wu, J.; Zhang, P. GO-modified double-walled polyurea microcapsules/epoxy composites for marine anticorrosive self-healing coating. *Mater. Des.* **2020,** 189.
36. Calado, L. M.; Taryba, M. G.; Carmezim, M. J.; Montemor, M. F. Self-healing ceria-modified coating for corrosion protection of AZ31 magnesium alloy. *Corros. Sci.* **2018,** 142, 12-21.
37. Cambon, J. B.; Ansart, F.; Bonino, J. P.; Turq, V. Effect of cerium concentration on corrosion resistance and polymerization of hybrid sol-gel coating on martensitic stainless steel. *Prog. Org. Coat.* **2012,** 75, (4), 486-493.
38. Della Rovere, C. A.; Alano, J. H.; Silva, R.; Nascente, P. A. P.; Otubo, J.; Kuri, S. E. Characterization of passive films on shape memory stainless steels. *Corros. Sci.* **2012,** 57, 154-161.
39. Fayomi, O. S. I.; Abdulwahab, M.; Popoola, A. P. I. Properties evaluation of ternary surfactant-induced Zn-Ni-Al_2O_3 films on mild steel by electrolytic chemical deposition. *J. Ovonic Res.* **2013,** 9, (5), 123-132.
40. Tuaweri, T. J.; Wilcox, G. D. Behaviour of Zn-SiO_2 electrodeposition in the presence of N,N-dimethyldodecylamine. *Surf. Coat. Technol.* **2006,** 200, (20-21), 5921-5930.
41. Popoola, A. P. I.; Fayomi, O. S. I.; Aigbodion, V. S.; Abdulwahab, M. Surface modification, strengthening effect and electrochemical comparative study of Zn-Al_2O_3-CeO_3 and Zn-TiO_2-CeO_3 coating on mild steel. *Int. J. Adv. Manuf. Technol.* **2016,** 85, (5-8), 1419-1427.
42. Shen, X.; Sheng, J.; Zhang, Q.; Xu, Q.; Cheng, D. The Corrosion Behavior of Zn/Graphene Oxide Composite Coatings Fabricated by Direct Current Electrodeposition. *J. Mater. Eng. Perform.* **2018,** 27, (7), 3750-3761.
43. Alagi, P.; Ghorpade, R.; Choi, Y. J.; Patil, U.; Kim, I.; Baik, J. H.; Hong, S. C. Carbon Dioxide-Based Polyols as Sustainable Feedstock of Thermoplastic Polyurethane for Corrosion-Resistant Metal Coating. *ACS Sustainable Chem. Eng.* **2017,** 5, (5), 3871-3881.